

Reactivity of a Morita–Baylis–Hillman Adduct Derivative Bearing a Triphenylamine Moiety with Lysine Models

Jacopo Venditti,^[a] Mario Saletti,^[a] Marco Paolino,^[a] Stefano Contena,^[a] Claudia Bonechi,^[a] Germano Giuliani,^[a] Gianluca Giorgi,^[a] Antonella Caterina Boccia,^[b] Chiara Botta,^[b] Lluís Blancafort,^[c] and Andrea Cappelli*^[a]

The reactivity of Morita–Baylis–Hillman Adduct (MBHA) derivative **7** was studied with different primary amine derivatives such as *n*-butylamine, *N* α -acetyl-*L*-lysine methyl ester, and a poly-(*L*-lysine) derivative as lysine models to obtain information about the possible reactions in complex protein environments. MBHA derivative **7** reacted with *n*-butylamine or *N* α -acetyl-*L*-lysine methyl ester producing monoadducts **9a** or **9c**, which showed bright emission features in the green region at 526–535 nm

with photoluminescence quantum yield values in solutions of 73% and 51%, respectively. Based on these results, MBHA derivative **7** can be considered an interesting new fluorogenic probe potentially useful in the labelling of basic amino acid residues. Furthermore, similar to other MBHA derivatives, compound **7** showed the tendency to produce diadducts especially in polar solvents system where specific interactions between the extended aromatic moieties may play a major role.

Introduction

Protein labeling currently represents one of the topics of increasing interest owing to its many applications including biosensing, diagnostic imaging, drug development, and targeted drug delivery.^[1] This is testified also by the numerous papers reporting the functionalization of proteins or antibodies, which could be useful as drugs versus cancer or infections.^[2] The techniques of protein labelling are primarily centered around methods involving the reaction of amino group of lysine or thiol groups of cysteine residues.^[3–8] Recently, Morita–Baylis–Hillman adduct (MBHA) derivatives were taken into account in protein labelling owing to the presence in their structure of an activated double bond susceptible to attack nucleophilic groups such as amino or thiol groups.^[9–18] The design of suitable probes has become a common motif in recent times in order to make them useful in protein labelling even in complex environments.^[19–21] For instance, the design of fluorescent labels has been the focus of increasing attention

owing to their potential usefulness in performing studies on protein interactions and function.^[22] In particular, a growing interest has been dedicated to the considerable advantages that characterize fluorogenic labeling techniques, which are capable of generating higher signal-to-noise ratio relying on fluorescence activation process following reaction/interaction with specific sites in the protein.^[22–24]

Another potential benefit of fluorogens can be the phenomenon called aggregation induced emission (AIE), in other words the ability to emit more in the solid state than in solution.^[25,26] Thanks to AIE, fluorogens can show greater photostability, accuracy, and sensitivity when compared to traditional probes that have remarkable emissive properties in solution but often suffer aggregation caused quenching (ACQ) processes at high concentration.^[27]

In this context, over the past few years, our research group developed some MBHA derivatives (i.e. compound **1**, Figure 1), which were able to react with imidazole^[10,11] or *n*-butylamine^[14] affording cinnamic derivatives (i.e. compounds **2**) showing fluorogenic characteristics.

With the aim of extending the π electron system, the substituted phenyl ring of MBHA derivatives **1** and **2** was replaced by naphthalene moiety leading to fluorogenic compounds (i.e. **3a,b**), which were found to react with imidazole with the formation of monoadducts or diadducts showing AIE features.^[11] Furthermore, the reactivity of the newly-designed naphthalene MBHA derivatives **3a,b** was investigated in model proteins. The interesting results obtained demonstrated the ability of **3a** to interact and functionalize lysine side chains in lipophilic pockets,^[14] while **3b** found applications in the PEGylation of poly-histidine tags of engineered proteins (Figure 1).^[12,13]

In the investigations focused on the optical features of polybenzofulvene derivatives,^[28–56] we were capable of recognizing cinnamic derivatives **4**, **5**, and **6** (Figure 2) as interesting fluorogenic compounds provided with photoluminescence

[a] J. Venditti, M. Saletti, M. Paolino, S. Contena, C. Bonechi, G. Giuliani, G. Giorgi, A. Cappelli
Dipartimento di Biotecnologie, Chimica e Farmacia, Università degli Studi di Siena, Via Aldo Moro 2, 53100 Siena, Italy
Tel: +39 0577 232416
E-mail: andrea.cappelli@unisi.it

[b] A. C. Boccia, C. Botta
Istituto di Scienze e Tecnologie Chimiche “G. Natta” - SCITEC (CNR), Via A. Corti 12, 20133 Milano, Italy

[c] L. Blancafort
Department of Chemistry, Institute of Computational Chemistry and Catalysis, University of Girona, C/ M. A. Capmany 69, 17003 Girona, Spain

Supporting information for this article is available on the WWW under <https://doi.org/10.1002/asia.202400617>

© 2024 The Authors. Chemistry - An Asian Journal published by Wiley-VCH GmbH. This is an open access article under the terms of the Creative Commons Attribution License, which permits use, distribution and reproduction in any medium, provided the original work is properly cited.

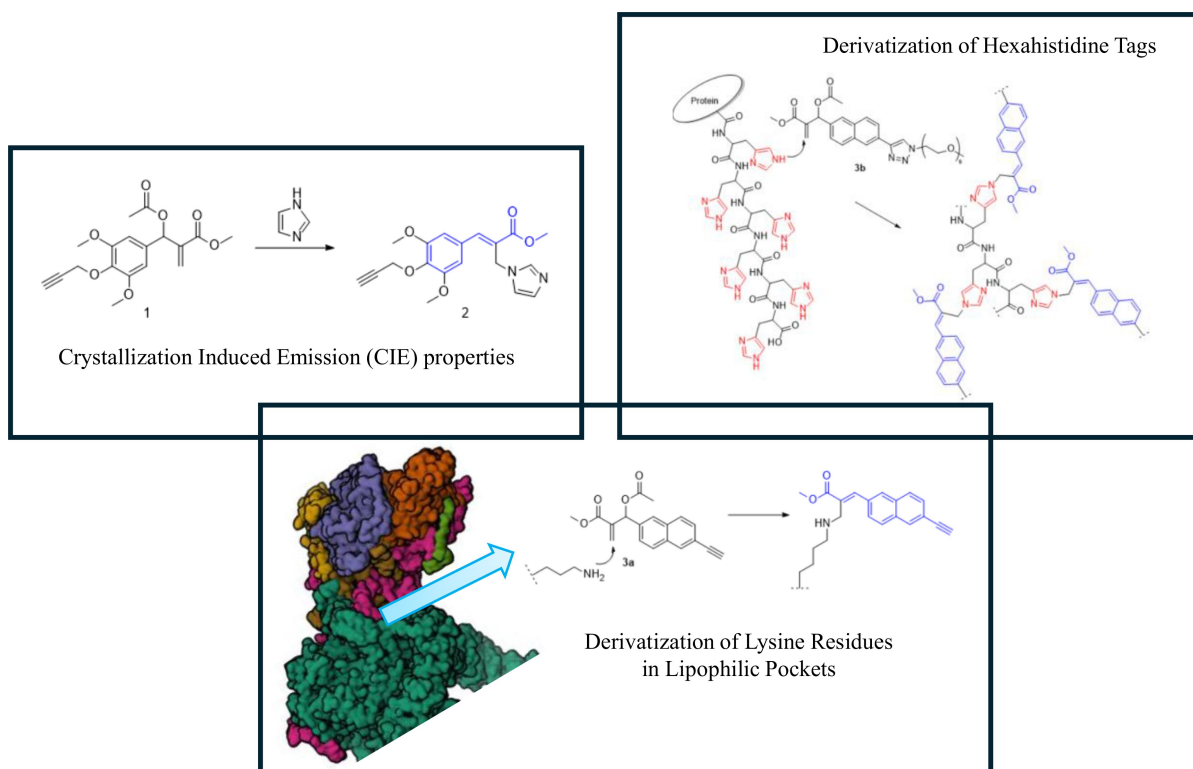


Figure 1. Structures of MBHA derivatives 1 leading to 2, and MBHA derivatives 3a,b involved in site-specific protein derivatization.

quantum yield (PL QY) values ranging from 57% to 80% and emission maxima in the range of 407–540 nm.^[57]

The promising findings obtained with triphenylamine derivative **6** stimulated the design of MBHA derivative **7**, which was synthesized and characterized from the point of view of its photophysical and photochemical features.^[15] Interestingly, the photophysical and photochemical characterization studies confirmed the promising properties of the cinnamic portion present in derivatives **6**, **11** and **12** (Figure 2).^[15] It is noteworthy that the shift of the double bond from the acrylic position (i.e. as in compounds **7** and **10**) to the cinnamic one of **6**, **11** and **12** compound produced a significant red-shift in the emission maxima of about 130–150 nm.^[15] MBHA derivative **7** was found to show intriguing AIE features since a bright blue emission (478 nm) was observed when its microaggregates were formed in DMSO-water dispersions.^[17] Moreover, **7** was found to react with human serum albumin (HSA) providing green fluorescent albumin (GFA) derivatives and switching its emission from the blue to the green-yellow (525 nm) in GFA.^[17] Docking studies were performed to evaluate the potential interaction of **7** with the lipophilic pockets present in HSA structure, and the obtained results proposed a possible interaction between the acrylic activated moiety with Lys199 driving to the addition-elimination reaction.^[17]

Thus, in the present work we investigated on the behaviour of **7** in reacting with *n*-butylamine, *N* α -acetyl-*L*-lysine methyl ester, and a poly-*L*-lysine derivative as models of the lysine amino acid residues. In our hypothesis, *n*-butylamine represented the simplest model of lysine residues, whereas *N* α -

acetyl-*L*-lysine methyl ester represented the isolated model of lysine residues, and the poly-*L*-lysine derivative represented the model of lysine inserted in the homopolymer.

Results and Discussion

Reactivity of MBHA Derivative **7** with Models of Lysine Residues

First, MBHA derivative **7** was tested in reactivity characterization studies with *n*-butylamine (pK_a = 10.8) as the simplest model of the basic amino acid residues lysine and the results are shown in Scheme 1.

Compound **7** reacted quickly with a large (i.e. five-fold) excess of *n*-butylamine in chloroform at room temperature. In particular, the reaction was almost complete after 6 h in agreement with the high nucleophilicity of *n*-butylamine, and provided monoadduct **9a** as the major reaction product (yield 66%) along with significant amount of diadduct **9b** (yield 13%). This result was found to be in full agreement with the ¹H NMR spectrum of the reaction mixture (Figure SI-1).

When the amount of butylamine was reduced from the large to a slight excess (i.e. 1.5:1) the reaction was found to slow down (i.e. it was almost complete after stirring at room temperature for 48 h), and the composition of the reaction mixture was found to be relatively different to that obtained in the large excess. In particular, the monoadduct **9a** was isolated in 49% yield, whereas the diadduct **9b** was obtained in 36%

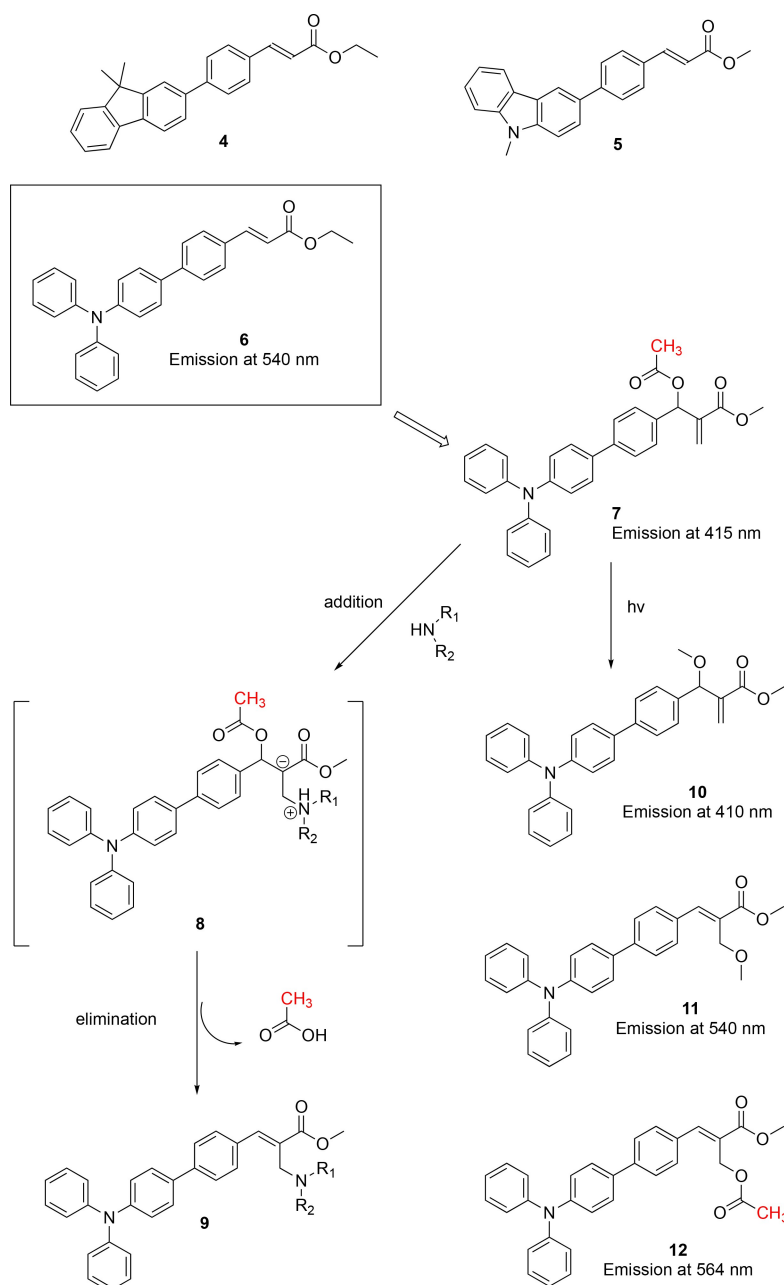


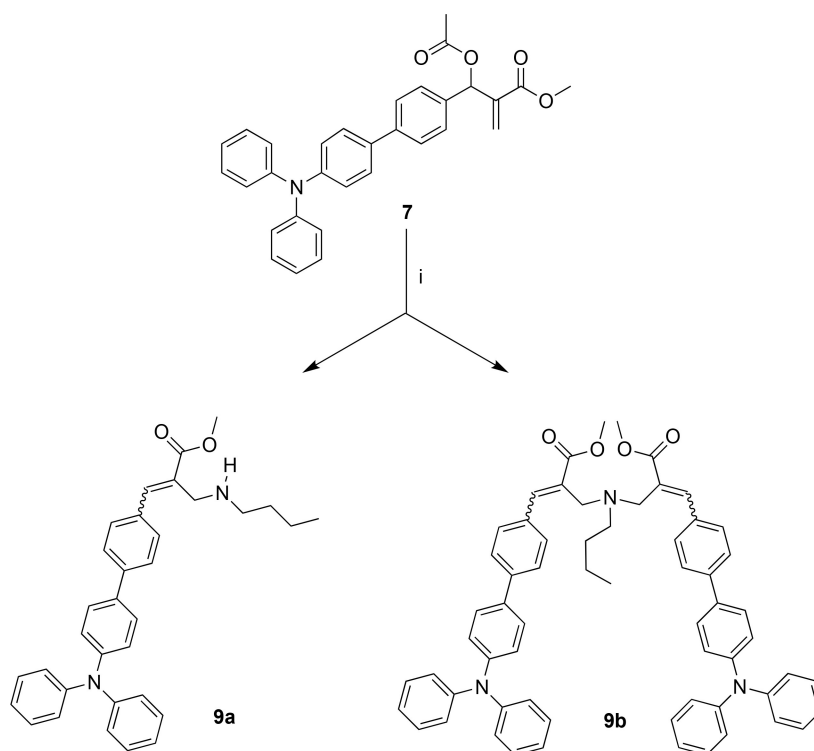
Figure 2. Structure of fluorescent cinnamic derivatives 4–6 and design of reactive MBHA derivative 7 leading to acrylic derivative 10 and cinnamic derivatives 9, 11, 12.

yield, in agreement with the ¹H NMR spectrum of the reaction mixture (Figure SI-2).

On the other hand, the reaction of 7 with *n*-butylamine hydrochloride in acetonitrile in the presence of phosphate buffered saline (PBS) solution at room temperature was very slow in agreement with the probable protonation state, which decreased its nucleophilicity. In fact, after stirring at room temperature for 24 h, only negligible amounts of MBHA derivative 7 were reacted. However, the heating of the reaction mixture at refluxing conditions allowed the completion of the reaction in reasonable time.

For example, the reaction of 7 with a large (i.e. five-fold) excess of *n*-butylamine hydrochloride was virtually complete after 24 h, and provided with the monoadduct 9a in 52% yield and the diadduct 9b in 39% yield according to the ¹H NMR spectrum of the reaction mixture (Figure SI-3).

Similarly, the reaction of 7 with a slight excess (i.e. 1.5:1) of *n*-butylamine hydrochloride was virtually complete after refluxing for 24 h. In this way, monoadduct 9a was isolated in 16% yield, while diadduct 9b was isolated as the main reaction product (i.e. yield 73%), in agreement with ¹H NMR spectrum of the reaction mixture (Figure SI-4).



Scheme 1. Reaction of MBHA derivative **7** with *n*-butylamine. Reagents: (i) *n*-butylamine, CHCl₃ (or *n*-butylamine hydrochloride, CH₃CN, H₂O, PBS).

Overall, these results confirmed the propensity of MBHA derivatives to produce diadducts.^[11,18] It is noteworthy that this propensity appeared more pronounced in polar solvent systems such as acetonitrile-water than in chloroform. This observation led to suspect that the driving force for the diadduct formation could be a specific interaction between the extended aromatic moieties of the fluorophores.

In order to obtain information about the reactivity of compound **7** with a more complex molecular system than *n*-butylamine, *N*α-acetyl-*L*-lysine methyl ester was selected as amino acid model (Scheme 2).

As expected, the reaction of compound **7** with a little excess (i.e. 1.5 equivalents) of *N*α-acetyl-*L*-lysine methyl ester hydrochloride in acetonitrile in the presence of phosphate buffered saline (PBS) at room temperature was very slow. Therefore, refluxing conditions were applied to carry out the reaction in reasonable times (i.e. 24 h). In this way, monoadduct **9c** was obtained in low yield (i.e. 14%), whereas diadduct **9d** represented the major reaction product and was isolated in 77% yield by flash chromatography separation of the reaction mixture, in agreement with the results obtained in the reaction of **7** with *n*-butylamine hydrochloride in the same conditions.

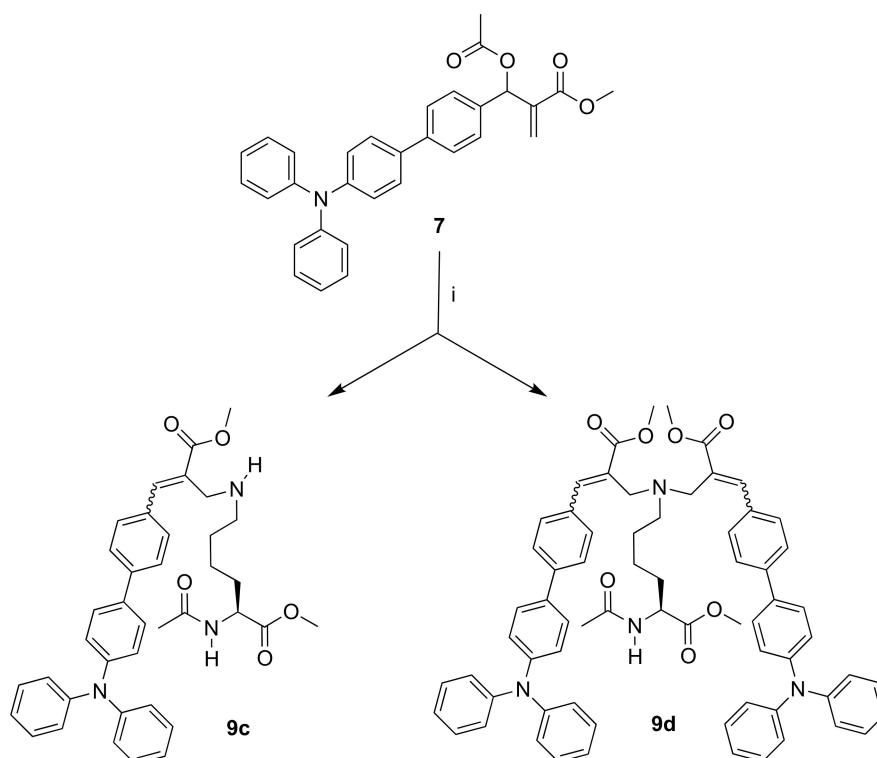
Finally, the reactivity of MBHA derivative **7** was evaluated by using *n*-butyl-poly-*(L)*-lysine (BPLL) hydrochloride (Iris Biotech GMBH) as the most complex model of lysine residues (Scheme 3).

The reaction was performed in deuterated DMSO in 5 mm NMR tubes to allow the reaction kinetics to be followed by ¹H NMR spectroscopy, and different excess (i.e. around 12:1, 6:1, and 3:1) of lysine residues were evaluated (Figures SI-5, SI-6, SI-

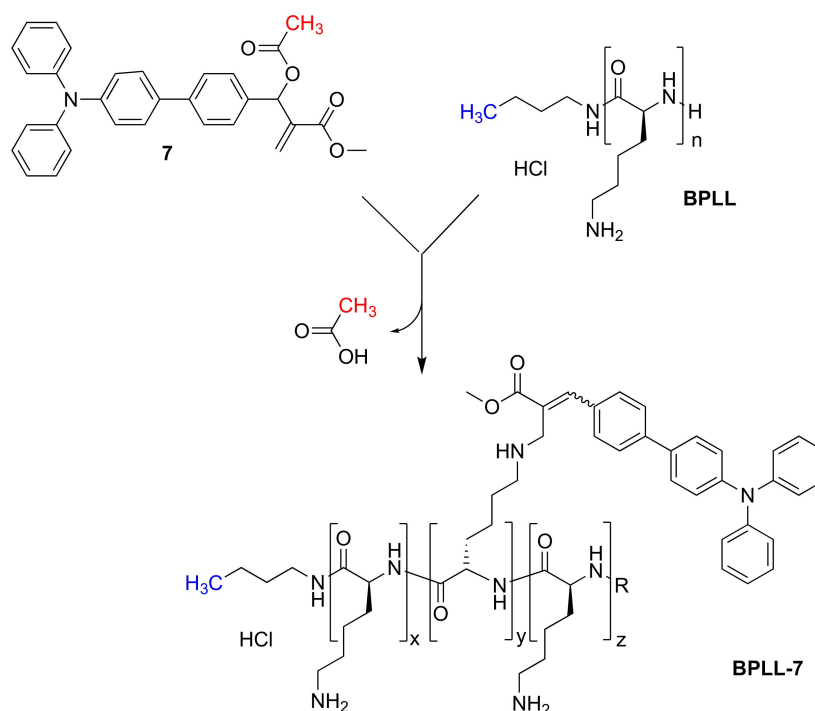
7). The reaction progress was evaluated by monitoring the decrease of the signal (at around 2.10 ppm) attributed to the methyl group of acetyl moiety of MBHA derivative **7**, and the appearance of the signal (at around 1.90 ppm) attributed to acetate, which was liberated during the reaction. The comparative analysis of the results suggested that the reaction was rather slow also at 50 °C and remained incomplete after 24 h also in the large excess of lysine residues.

The same experiments were then repeated in the presence of suitable amounts of DIPEA as the base (Figures SI-8, SI-9, SI-10). As expected, the presence of DIPEA played a crucial role allowing the reaction to go rapidly to completion also in the case of low excess of lysine residues (Figure SI-10) that led to highly conjugated poly-*(L)*-lysine derivatives.

These results highlighted the importance of the protonation state of lysine residues in the reaction with MBHA derivative **7**. Owing to the probable protonation state of the solvent-exposed lysine derivatives, compound **7** could be proposed as a selective reagent for nucleophilic amino acid residues embedded into lipophilic pockets of suitable accessibility. As suggested by the examination of the 3D-structure of water-soluble proteins such as HSA obtained by crystallographic studies, the lysine residues located inside the protein structure establish charge assisted H-bond interactions with suitable counterparts, which can produce an increased nucleophilicity and therefore an increased reactivity. Moreover, the initial binding recognition step could be determinant in governing reactivity and selectivity of MBHA derivatives towards proteins. In other words, the suitable binding affinity and orientation in the pocket containing the reactive amino acid residue could



Scheme 2. Reaction of MBHA derivative **7** with $N\alpha$ -acetyl-*L*-lysine methyl ester. Reagents: (i) $N\alpha$ -acetyl-*L*-lysine methyl ester hydrochloride, CH_3CN , PBS, H_2O .



Scheme 3. Reaction of MBHA derivative **7** with *n*-butyl-poly-(*L*-lysine) (**BPLL**). Reagents: (i) DMSO-d_6 .

play a key role in producing the desired selectivity. Finally, we assume that in the context of the reaction of MBHA derivatives with reactive amino acid residues embedded into lipophilic

pockets, the propensity to the formation of diadducts should be largely reduced.

Structure of of Monoadduct **9a** and Diadduct **9b**

The structure of the major diastereomer of monoadduct **9a** was studied along with that of the major diastereomer of diadduct **9b** by NMR spectroscopy, molecular modeling, and mass spectrometry techniques.

The purity of the samples used in the structural characterization was evaluated by RP-HPLC with the following experimental set-up: a column ZORBAX eclipse XDB-C8 4.6×150 mm 5 μm; an isocratic elution with a ternary solvent mixture composed by 70% methanol, 20% acetonitrile, and 10% water containing 0.2% formic acid; flow = 1.25 mL/min; analysis time = 10 min.

The purity of monoadduct **9a** was found higher than 94% with the main impurity being the corresponding minor diastereomer, while the purity of diadduct **9b** was around 80% in all the batches synthesized, with the minor diastereomers being the main impurities.

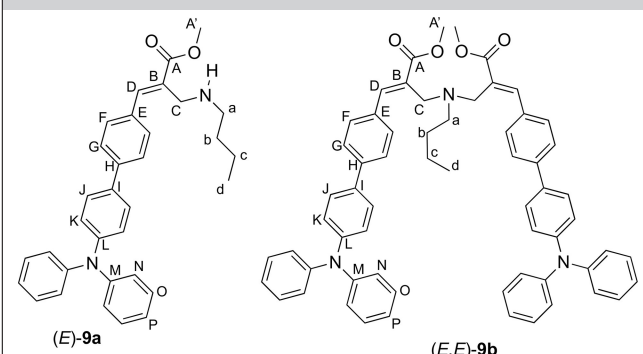
The stability of **9a,b** solutions in DMSO was evaluated by ¹H NMR spectroscopy. The ¹H NMR spectra performed (in DMSO-d₆) after storage of the solutions at room temperature for one week were perfectly consistent with those performed immediately after the preparation. Similarly, the stability as glassy solids stored in closed vials at room temperature (for more than one month) was confirmed by ¹H NMR spectroscopy.

The presence of a cinnamic fluorophore in structure of monoadduct **9a** could lead to the possible existence of two geometric isomers showing (*E*) and (*Z*) configurations. The results of NMR studies suggested for the most abundant isomer **9a** a three-dimensional (3D) structure with the cinnamic moiety showing the trans (*E*) configuration at the double bond, as supported by the chemical shift value of the acrylic proton (D). On the other hand, the presence of two cinnamic fluorophores in structure of diadduct **9b** could lead to the possible existence of three geometric isomers, namely (*E,E*), (*E,Z*), and (*Z,Z*). The NMR spectrum suggested for the most abundant isomer **9b** a highly symmetric three-dimensional (3D) structure, with the two cinnamic moieties showing the trans (*E*) configuration at the double bond, as supported by the chemical shift value of the acrylic proton (D). Owing to both the relative complexity of the NMR spectrum and the relatively low amounts, the minor diastereomers of **9b** were not taken into consideration in the NMR studies.

The structures of (*E*)-**9a** and (*E,E*)-**9b** were assigned by NMR experiments and by crossing mono- and two-dimensional data. The characteristic chemical shift values of the carboxylic ester groups [167.9 ppm in (*E*)-**9a** and 168.4 ppm in (*E,E*)-**9b**] were used as the starting points in the assignment of the olefinic proton D [signals at 7.70 ppm (140.2 ppm) in (*E*)-**9a** and 7.75 ppm (141.3 ppm) in (*E,E*)-**9b**] and the adjacent methylene protons (C) at 3.49 ppm (45.4 ppm) in (*E*)-**9a** and 3.49 ppm (49.8 ppm) in (*E,E*)-**9b**, according to the ¹H-¹³C correlations in the HMBC spectrum (Table 1).

Interestingly, the comparison of the chemical shift values shown by diadduct (*E,E*)-**9b** with the corresponding ones of monoadduct (*E*)-**9a** showed the existence of up-field shifts in the signals attributed to protons G, J, O, P, N, and K (Figure 3).

Table 1. Assignment of NMR signals of monoadduct (*E*)-**9a** and diadduct (*E,E*)-**9b**.



	(<i>E</i>)- 9a DMSO-d ₆		(<i>E,E</i>)- 9b DMSO-d ₆	
	¹ H (ppm)	¹³ C (ppm)	¹ H (ppm)	¹³ C (ppm)
b	1.39	31.3	1.39	27.5
c	1.31	19.9	1.15	20.1
d	0.86	13.8	0.77	13.8
a	2.54	48.7	2.39	53.3
C	3.49	45.4	3.49	49.8
A'	3.75	51.9	3.68	51.9
K	7.03	122.9	6.95	122.7
N	7.06	124.3	7.02	124.3
P	7.07	123.4	7.05	123.4
O	7.33	129.6	7.30	129.6
G	7.70	126.0	7.51	125.8
J	7.65	127.6	7.52	127.6
F	7.70	130.5	7.71	131.2
D	7.70	140.2	7.75	141.3
A		167.9		168.4
B		129.6		129.3
E		133.2		133.1
H		140.0		140.0
I		132.8		132.6
L		147.1		147.1
M		146.9		146.8

This observation suggested the existence of specific interactions between the aromatic moieties in the structure of diadduct (*E,E*)-**9b**.

This assumption was also evaluated in the light of the dipolar correlations observed in NOESY experiments, which provided us with the information on the dipolar connectivity shown in Table 2.

The most important information from the comparative analysis of NOESY spectra was that an apparent dipolar interaction between the protons F and a was observed in diadduct (*E,E*)-**9b**. This observation suggested a possible interaction (in the 3D space) of the butyl sidechain with the cinnamic fluorophore in spite of their apparent distance in the

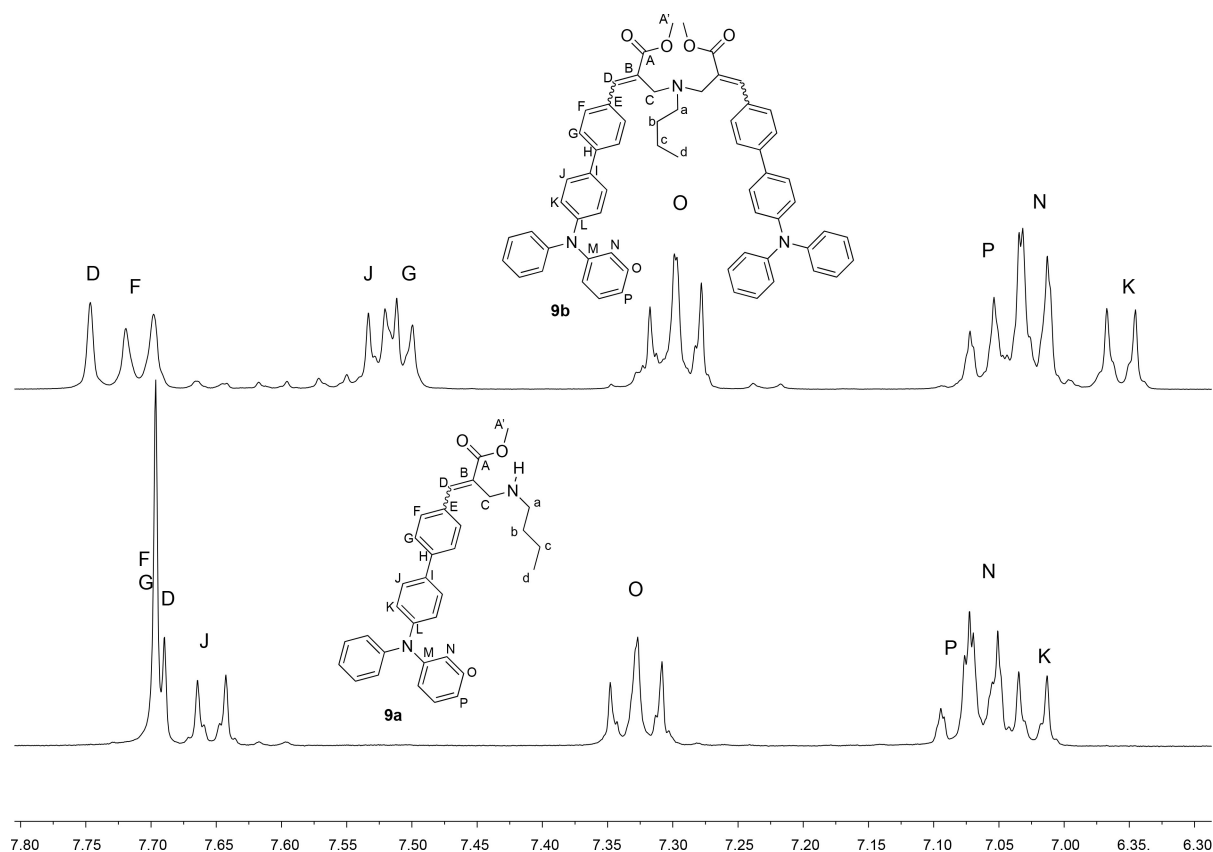


Figure 3. Comparison of the aromatic region of ^1H NMR (400 MHz, DMSO-d_6) spectrum of monoadduct **9a** and diadduct **9b**. The up-field shifts observed in the signals attributed to protons G, J, O, P, N, and K support the establishment of specific interactions between the aromatic moieties in the diadduct **9b**.

molecule. On the other hand, only obvious dipolar interactions were observed in the NOESY spectrum of mono adduct **9a**.

Overall, the results of the NMR studies provided evidence on the compactness of the 3D structure of diadduct (*E,E*)-**9b** that was stabilized by the establishment of stacking interactions between its extended aromatic moieties.

Owing to the structural information obtained by the NMR studies, the (*E,E*)-stereoisomer of **9b** was chosen as the starting geometry for the optimizations in DMSO. The results obtained are shown in Figure 4.

The calculations suggested a structure with the aromatic moieties arranged into a π - π stacking due to the non-covalent interactions between the π bonds of the aromatic rings. If we consider the molecular orbitals shown in Figure 5, in addition to the typical π -conjugation on the aromatic substituents, the orbital overlap caused by the stacking of aromatic rings can be easily identified in both ground and excited states.

Once the most probable structure of (*E,E*)-**9b** was determined, we focused our attention on its theoretical spectroscopic features in both DCM and DMSO as implicit solvents.

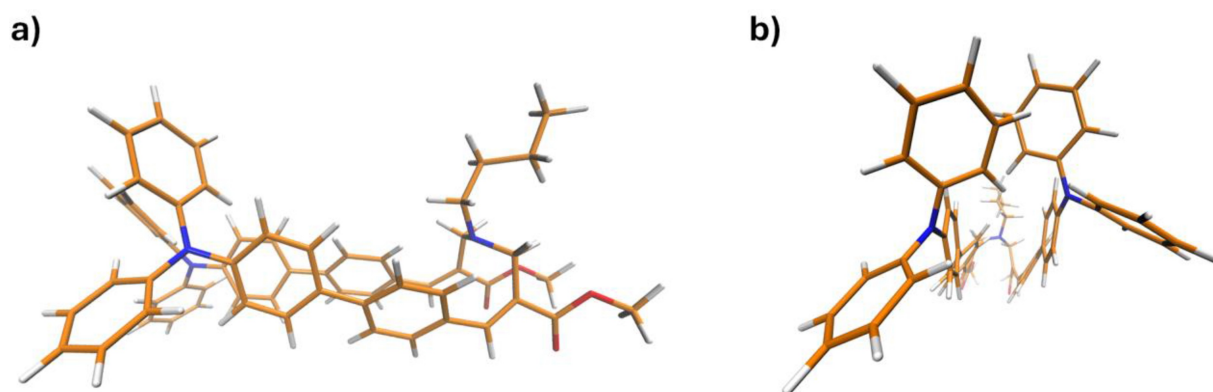
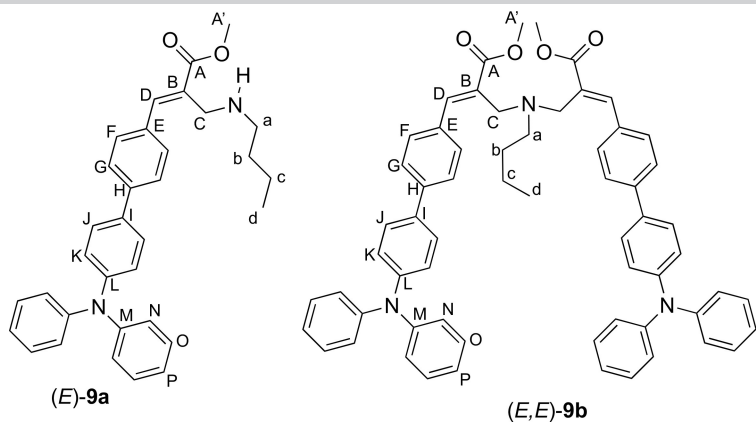


Figure 4. Optimized ground state structure of (*E,E*)-**9b** in DMSO as the solvent. (a) Side view and (b) front view.

Table 2. Dipolar correlations in monoadduct (*E*)-**9a** and diadduct (*E,E*)-**9b** obtained by NOESY experiments performed in DMSO-*d*₆.



Cross-peak volume

Proton	Proton	(E)- 9a			(E,E)- 9b		
		Small	Medium	Large	Small	Medium	Large
D	C					X	
D	a				X		
F	C						x
F	a					X	
F	b				X		
C	a						x
C	d					X	
C	b						x
a	d				X		
a	b			x	X		
c	d			x			
J	C					X	
J	a				X		
J	b				X		
J	K			x			
O	P			x			
O	N			x			

Figure 5 shows the geometries obtained of the ground state (S_0), the Frank-Condon point (FC), the first excited state singlet emitter (S_1), and the distorted ground state after radiative relaxation, in DCM. The simulations of **9b** were also carried out in DMSO and the results are reported in the Supporting Information (Figure SI-11). As can be seen, the change of solvent does not show any effect on the spectroscopic properties of the molecule, and this is likely due to the lipophilicity of its aromatic and aliphatic chains. Indeed, the effects of solvents on the spectroscopic properties of molecules (solvatochromism) are often driven by affinity between solute and solvent, such as the polarity of the solvents and the ability to form hydrogen bonds with the solute.^[58,59] In our case, the spectroscopic properties of the strong lipophilic compound **9b** appear to be unaffected by the substitution of polar aprotic solvents (DMSO/DCM).

Anyway, for each structure the HOMO/LUMO molecular orbitals involved in the electronic transition and the relative energy gap are reported. By comparison of the experimental data (see below Table 3) with the calculated ones, a good correlation regarding the absorption energy values can be noted. Specifically, the vertical excitation wavelength computed at the FC point in DCM (3.7 eV or 336 nm) shows a slight blue-shift with respect to the experimentally observed one (3.5 eV or 356 nm).

Starting from the FC structures, adiabatic relaxation on the first excited state S_1 was simulated (red arrows in Figure 5) to obtain geometries and relative wavelengths of the emitting intermediates. Comparing the values of Table 3 and of Figure 5, the calculation shows an emission energy in good agreement with the experimental one (2.35 eV or 528 nm and 2.33 eV or 532 nm). As previously mentioned, in DMSO the calculated

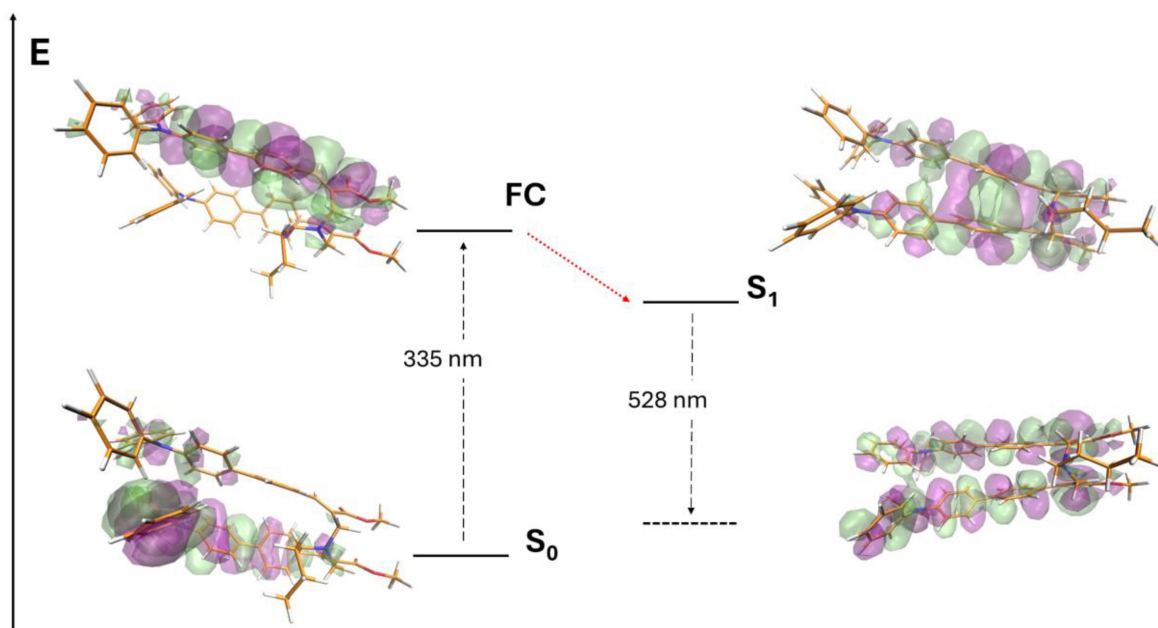


Figure 5. Schematic representations of (*E,E*)-**9b** fluorescence cycle in DCM. The molecular orbital (HOMO/LUMO) involved in electron transitions and relative energies, are shown for vertical excitation (Frank-Condon point, FC) and emission, from the optimized geometries. The red line stands for the adiabatic relaxation pathway on first singlet excited state (S_1).

Table 3. Comparison of the optical properties of compounds **9a–d** and **13** with those of model cinnamic derivative **6**, **11**, and **12** (see reference 15).

	Solution[a]			Solid-state			
	λ_{ab} (nm)	λ_{em} (nm)	QY ^[b] (%)	τ ^[c] (ns)	λ_{em} (nm)	QY ^[d] (%)	τ_{av} ^[e] , ^[f] (ns)
9a	290, 363	526	73	3.05	485	45	2.05
9b	295, 359	405	29 ^[f]	1.56 ^[*]	480	16	1.58
		526	13	1.42 ^[§,¶]			
9c	296, 357	535	51	3.38 ^[¶]	530	5	1.44
9d	296, 356	408	43 ^[f]	1.6 ^[*]	520	13	2.11
		524	29	2.82 ^[§,¶]			
13	331	406	43 ^[f]	1.60	450	39	1.96
6	292, 371	540	78	3.32	470	80	3.02
7	330	415	3	0.35			
10	242, 332	411	2	0.41	440	41	2.89
11	292, 362	540	75	3.36	485	46	3.00
12	290, 367	564	58	3.52	504	43	2.61

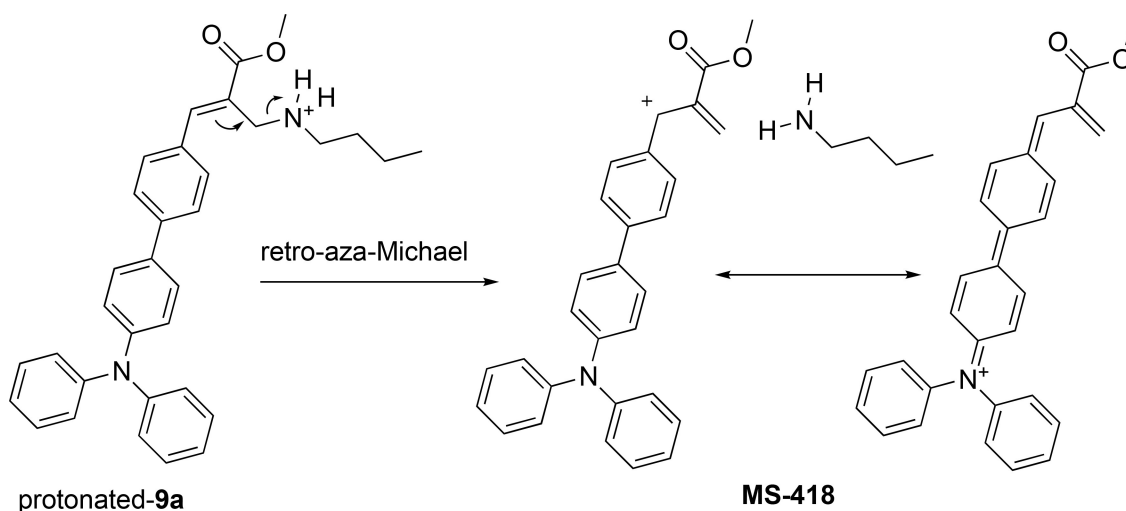
[a] dichloromethane, [b] λ_{ex} = 365 nm; [c] λ_{ex} = 300 nm, [d] λ_{ex} = 390 nm, [e] λ_{ex} = 407 nm, [f] λ_{ex} = 330 nm; τ = lifetime from mono-exponential decay fit; τ_{av} = average lifetime $\tau_{av} = \frac{\sum_{n=1}^m A_n \tau_n^2}{\sum_{n=1}^m A_n \tau_n}$ [°] from bi-exponential fit, [°] from three-exponential fit; [*] λ_{em} = 406 nm; [§] λ_{em} = 526 nm.

spectroscopic results are comparable to those in dichloromethane (see Figure SI-11).

Mass spectrometry studies performed on monoadduct **9a** with a mass spectrometer (Agilent 1100 LC/MSD) equipped with an electrospray source (ESI) revealed the presence of a peak at m/z 491 attributed to the protonated molecule (representing the base peak of the spectrum) along with another high intensity peak at m/z 418, which was assumed to be produced by a retro-aza-Michael reaction of **9a** protonated molecule (Scheme 4).

This result suggested a certain degree of lability of the bond connecting the cinnamic fluorophore to the butylamine nitrogen owing to the apparent high stability of the fragment showing a mass value of m/z 418. It should be noted that the positive charge could be stabilized by resonance over the entire structure of the fragment.

On the other hand, the mass spectrum obtained with diadduct **9b** showed the presence of a peak at m/z 908 attributed to the protonated molecule along with some other low intensity peaks, suggesting the higher stability of diadduct



Scheme 4. Mechanistic hypothesis for the fragmentation of compound 9a.

9b with respect to monoadduct 9a in the gas phase conditions of the mass spectrometry experiments. Similar results were obtained by the high resolution mass spectrometry measurements performed with a timsTOF spectrometer (Bruker, Bremen, D) equipped with an electrospray source (ESI).

Photophysical Properties of the Newly Synthesized Compounds

We previously reported that cinnamic derivative 6 showed an emission maximum at 540 nm with photoluminescence quantum yield (PL QY) values of 78% in solution and of 80% in the crystalline state.^[57] Therefore, these outstanding photophysical properties stimulated the development of MBHA derivative 7,^[16,17] which was very reactive towards *n*-butylamine (see

above). Thus, the corresponding cinnamic derivatives 9a,b were characterized from the point of view of their photophysical features.

At first sight, the optical features of monoadduct 9a in solution were very promising and similar to those shown by models cinnamic derivative 6, which share the same fluorophore. In particular, compound 9a showed a significant emission spectrum in dichloromethane solution at low concentration values that was characterized by a large asymmetric peak with a maximum at 526 nm (Figure 6, left) and a PL QY value of 73%.

On the other hand, a double component emission was observed in the PL spectrum of diadduct 9b (Figure 6, right), suggesting the presence of two emitting species in solution. In fact, the relative intensities of the two components were excitation dependent (see the spectra at three different

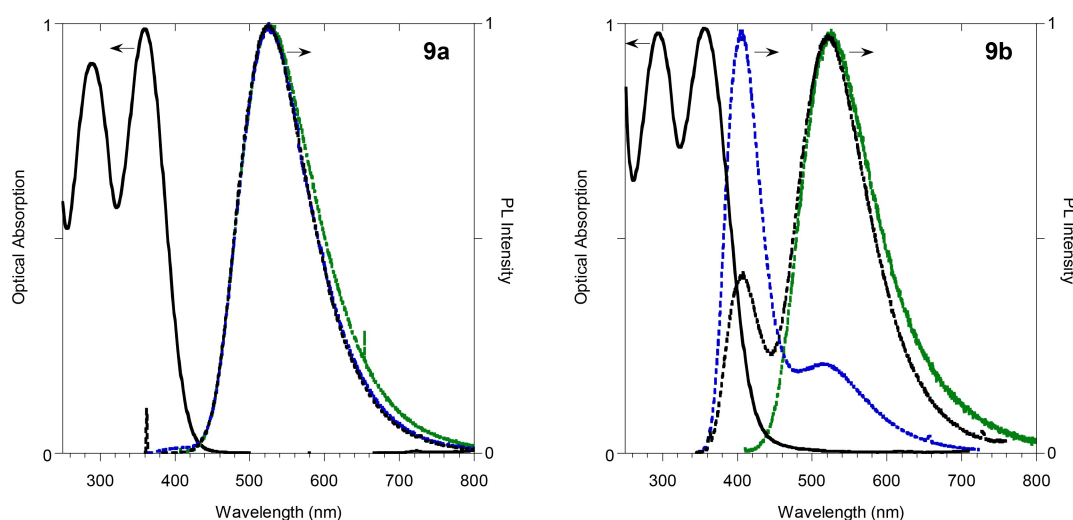


Figure 6. Normalized absorption (black solid line) and PL spectra (dashed lines) of monoadduct 9a (left) and diadduct 9b (right) in dichloromethane solutions at different excitation wavelengths (330 nm, blue; 365 nm, black; 408 nm, green). The measurements are performed with freshly prepared solutions at about 10^{-5} M concentrations.

excitation wavelengths in Figure 6, right). In particular, **9b** showed a low energy component at around 526 nm coincident with the emission spectrum of monoadduct **9a** and a high energy component (at around 405 nm), not related with the emission of the **9b** structure (see Figure SI-12), suggesting the possible formation of a new chemical entity responsible for the high energy emission.

Very interestingly a similar behavior was observed in the couple of structurally related monoadduct **9c** and diadduct **9d** (Figure 7).

In fact, the results obtained with the lysine derivatives **9c,d** confirmed the bright emission features of monoadduct derivative **9c** at 535 nm (PL QY = 51%) in dichloromethane and the double emission of the diadduct derivative **9d** with the low energy component at 524 nm and the high energy component at 408 nm. Also in this case the high energy emission appeared to be not related with the low energy component and with the structure (see the different excitation profiles in Figure SI-13), of **9d** advocating the possible formation of a new chemical entity responsible for the high energy emission. Therefore, we assumed that the high energy peaks at around 405–408 nm could be generated by the products of the [2+2] photocycloaddition promoted by the excitation (see the Photochemical Properties section below).

The photophysical features of compounds **9a–d**, and **13** are summarized in Table 3 for both the solid state (i.e. solid casted films) and the solutions and compared with those of the previously reported model compounds **6**, **7**, **10**, **11**, and **12** (see Table 3).^[15]

The comparison of the photophysical properties of the whole series of compounds both in solution and in the solid state allows us to draw some important conclusions. First, the similarity of the emission observed for compounds **9a** and **9c** to that of compound **6** in solution suggests its assignment to the common cinnamic derivative. Secondly, the high energy emission component observed at 405–408 nm for compounds

9b and **9d** suggests the occurrence of a photochemical reaction leading to similar photoproducts, as discussed in the next section. In the solid state, due to the higher stability of the compounds and the efficient migration processes to the lower energy emitting states, compounds **9a** and **9b**, as well as **9c** and **9d**, display the same emission position at about 480 nm and 520 nm, respectively.

Photostability of Compounds **9a,b**

Further characterization studies were then performed on compounds **9a,b** in order to assess their potential photostability. On the basis of the UV-vis absorption spectra, the solutions of the two compounds in deuterated dichloromethane were irradiated with monochromatic light centered at either 365 nm or 420 nm to probe their reactivity, and this was followed via ¹H NMR spectroscopy by recording spectra at regular time intervals (i.e. 0 min, 15 min, 30 min, 1, 2, 4, 8, and 24 h).

First, a solution of **9a** in deuterated dichloromethane (ca. 1.4×10^{-2} M) contained into a 5 mm NMR Pyrex tube was irradiated with monochromatic light centered at either 365 nm or 420 nm until a photo-stationary state was reached. Interestingly, compound **9a** showed a high photostability in these conditions since the irradiation produced only a slight change in the composition of the diastereomeric *E/Z* mixture. In particular, we observed a very small change in the composition of the diastereomeric *E/Z* mixture from (90:10) to (93:7) (Figure SI-14) at 365 nm, and a variation from (90:10) to (80:20) (Figure SI-15) at 420 nm. This *E/Z* ratio was obtained from the integral values of the signals attributed to the same protons in the two diastereomeric species. In particular, the formation of (*Z*)-**9a** was supported by the increase in intensity of the H–D signal at 6.85 ppm, the H–A' signal at 3.73 ppm, and H–C signal at 3.62 ppm.

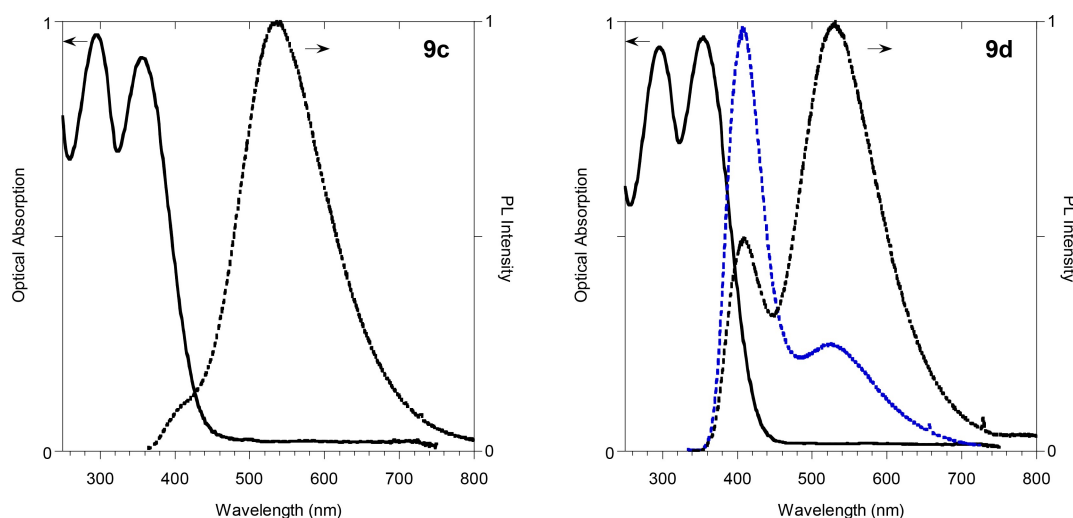
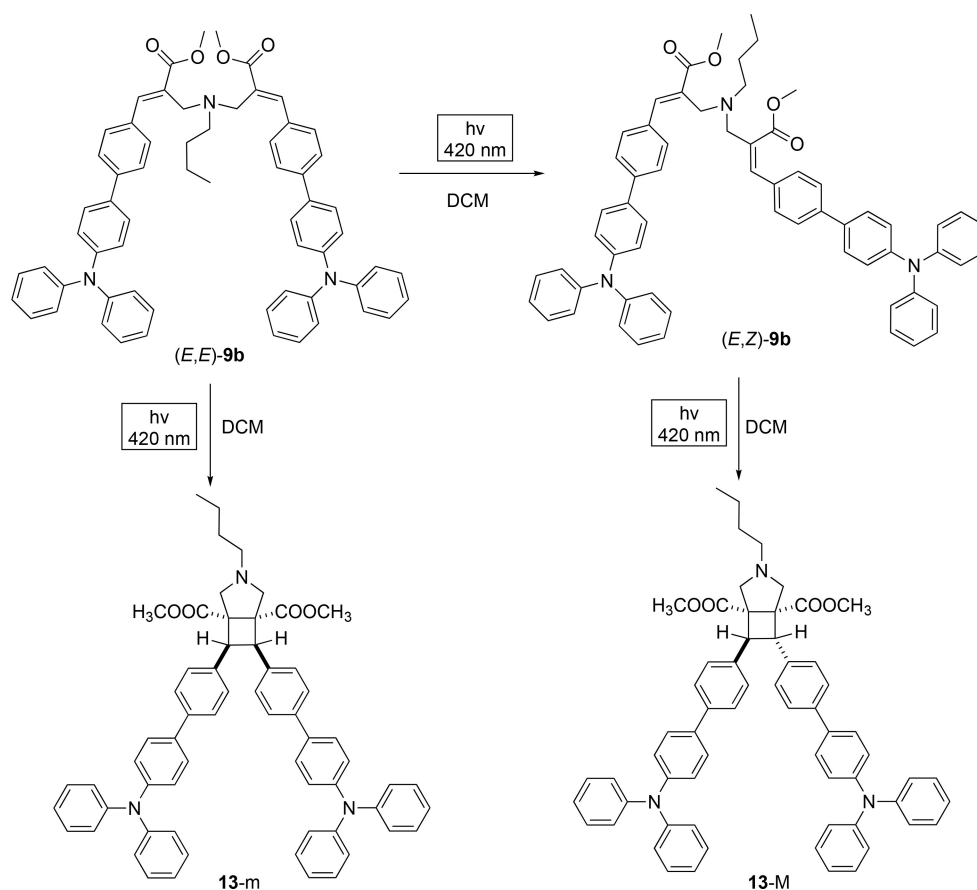


Figure 7. Normalized absorption (black solid line) and PL spectra (dashed lines) of monoadduct **9c** (left) and diadduct **9d** (right) in dichloromethane solutions at different excitation wavelengths (330 nm, blue; 365 nm, black). The measurements are performed with freshly prepared solutions at about 10^{-5} M concentrations.



Scheme 5. [2 + 2] Photocycloaddition of compound 9b leading to 13.

Despite the high photostability shown by monoadduct 9a, the irradiation of diadduct 9b in the same conditions led to the formation of several chemical species as indicated by the ^1H NMR analysis (Figures SI-16 and SI-17). At the preparative scale it was possible to isolate compound 13-M as the main photoproduct (Scheme 5). This product results from a [2 + 2] photocycloaddition between the double bonds of the two cinnamic acid groups, leading to a cyclobutane ring. This photochemical process is allowed by the Woodward-Hoffmann rules and has been well studied, for instance, in thymine derivatives.^[60] The frontier molecular orbitals of 9b at the S_1 minimum (right hand side of Figure 5) display antibonding interactions between the orbitals of the two π systems in the HOMO and bonding interactions in the LUMO, which is similar to what is found in a pair of π stacked thymine molecules. This supports our mechanistic assignment.

The characterization of the optical features of 13 confirmed the emission properties this compound (Figure 8) with a very intense band at around 406 nm with a PL QY value of 43% in dichloromethane solutions and a lifetime value of 1.60 ns, in agreement with the results obtained for the high energy emission component of 9b and 9d (see Table 3). Interestingly, compound 13 was obtained as a white solid retaining the emission features also in the solid state. For instance, in the film

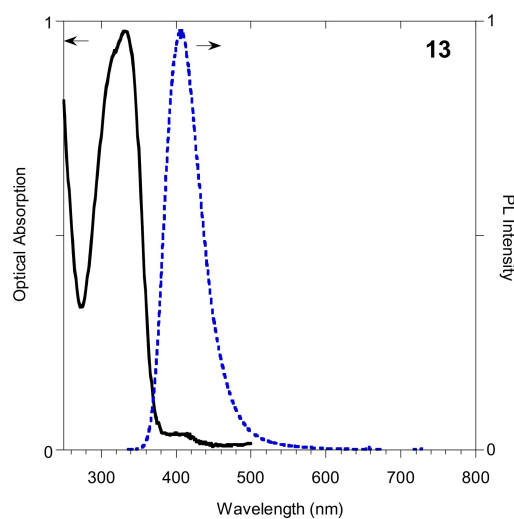


Figure 8. UV-visible absorption (black solid line) and PL spectrum (dashed blue line, excitation at 330 nm) of compound 13 in dichloromethane solution. The concentration values were 10^{-5} M for the absorption spectrum and 10^{-8} M or 10^{-7} M for the emission spectrum.

cast from dichloromethane we observed a red shifted emission at 450 nm with a PL QY value of 39%.

The comparison of Figure SI-16 with Figure SI-17 suggested that compound 13 appeared to be rather photostable against

irradiation at 420 nm, whereas apparent decomposition signs appeared when irradiated at 365 nm. Notably, the absence of absorption at 420 nm in the spectrum of compound **13** explained the observed photostability against visible irradiation, which can be used to profitably convert diadduct **9b** to compound **13**.

Conclusion

Motivated by the postulated reaction with a lysine residue into a lipophilic pocket of the human serum albumin, the reactivity of MBHA derivative **7** was studied with *n*-butylamine, *N* α -acetyl-*L*-lysine methyl ester, and a poly-*(L*-lysine) derivatives as lysine models to obtain information about the possible reactions in complex protein environments.

The results obtained in the present work stressed the importance of the protonation state of lysine residues in the reaction with MBHA derivative **7**. Owing to the probable protonation state of the solvent-exposed lysine derivatives, compound **7** could be proposed as a selective reagent for nucleophilic amino acid residues embedded into lipophilic pockets of suitable accessibility. As suggested by the examination of the 3D-structure of water-soluble proteins such as **HSA** obtained by crystallographic studies, the lysine residues located inside the protein structure establish charge assisted H-bond interactions with suitable counterparts, which can produce an increased nucleophilicity and therefore an increased reactivity. Moreover, the initial binding recognition step could be determinant in governing reactivity and selectivity of MBHA derivatives towards proteins. In other words, the suitable binding affinity and orientation in the pocket containing the reactive amino acid residue could play a key role in producing the desired selectivity.

The reaction of MBHA derivative **7** with *n*-butylamine or *N* α -acetyl-*L*-lysine methyl ester produced monoadducts **9a** or **9c**, respectively, both showing bright emission features (526 nm and 535 nm, respectively) in the same range of the one observed with green-fluorescent **HSA** (i.e. 525 nm),^[17] and PL QY values in solutions of 73% and 51%, respectively. This result places MBHA derivative **7** in an outstanding position as a new fluorogenic probe potentially useful in the labelling of basic amino acid residues.

Moreover, the peculiar reactivity shown by MBHA derivative **7** confirmed the tendency of MBHA derivatives to produce diadducts, and this tendency appeared more pronounced in polar solvent systems (i.e. acetonitrile-water). This observation led us to consider the specific interactions between the extended aromatic moieties of diadduct (*E,E*)-**9b** fluorophores as the driving force for the diadduct formation, and the results of the NMR studies supported the existence of these specific interactions. However, in the context of the reaction of MBHA derivatives with reactive amino acid residues embedded into lipophilic pockets, the propensity to the formation of diadducts should be largely reduced.

Experimental Section

Synthesis

Merck silica gel 60 (230–400 mesh) was used for column chromatography. Merck TLC plates, silica gel 60 F₂₅₄ were used for TLC. NMR spectra were recorded with a Bruker DRX-400 AVANCE III or a Bruker DRX-600 AVANCE III spectrometer in the indicated solvents (residual peak of the solvent as the internal standard): the values of the chemical shifts are expressed in ppm and the coupling constants (*J*) in Hz. An Agilent 1100 LC/MSD operating with an electrospray source (ESI) in positive ion mode was used in mass spectrometry experiments. On the other hand, high resolution mass spectra (HRMS) were obtained by using a timsTOF spectrometer (Bruker, Bremen, D) operating with an electrospray ionization source (ESI) in positive ion mode.

Reaction of MBHA Derivative **7** with *n*-butylamine in Chloroform

Large Excess of *n*-butylamine

A mixture of MBH acetate **7** (50 mg, 0.105 mmol) in chloroform (10 mL) containing *n*-butylamine (0.052 mL, 0.525 mmol) was stirred at room temperature for 6 h. The reaction mixture was concentrated under reduced pressure and the resulting residue was purified by flash chromatography with the appropriate eluents to obtain the amine derivatives reported below (**9a,b**).

Dimethyl 2,2'-((butylazanediyl)bis(methylene))bis(3-(4'-(diphenylamino)-[1,1'-biphenyl]-4-yl)acrylate) (**9b**)

Compound **9b** was obtained as a yellow glassy solid (6.0 mg, yield 13%) by using petroleum ether-ethyl acetate (9:1) as the eluent in the above flash chromatography purification. The ¹H NMR (400 MHz, DMSO-*d*₆) spectrum showed that compound **9b** was composed by a mixture of the diastereomers. Samples of major diastereomer (*E,E*)-**9b** showing higher purities were obtained by further purification by flash chromatography. ¹H NMR (600 MHz, DMSO-*d*₆): 0.77 (t, *J* = 7.3, 3H), 1.15 (m, 2H), 1.39 (m, 2H), 2.39 (t, *J* = 7.2, 2H), 3.49 (s, 4H), 3.68 (s, 6H), 6.95 (d, *J* = 8.5, 4H), 7.02 (d, *J* = 7.9, 8H), 7.05 (m, 4H), 7.30 (t, *J* = 7.7, 8H), 7.52 (m, 8H), 7.71 (d, *J* = 8.2, 4H), 7.75 (s, 2H). HRMS (timsTOF) *m/z*: [M + H]⁺ Calcd for C₆₂H₅₈N₃O₄ 908.44218; Found 908.43915.

Methyl 2-((butylamino)methyl)-3-(4'-(diphenylamino)-[1,1'-biphenyl]-4-yl)acrylate (**9a**)

Compound **9a** (34 mg, yield 66%) was obtained as a yellow glassy solid as the most polar fraction by using petroleum ether-ethyl acetate (7:3) as the eluent in the above flash chromatography purification. The ¹H NMR (400 MHz, DMSO-*d*₆) spectrum showed that compound **9a** was composed by a mixture of (*E/Z*)-diastereomers in the ratio of about (74:26). Samples of major diastereomer (*E*)-**9a** showing higher purities were obtained by further purification by flash chromatography. ¹H NMR (400 MHz, DMSO-*d*₆) 0.86 (t, *J* = 7.2, 3H), 1.24–1.45 (m, 4H), 2.53 (t, *J* = 6.8, 2H), 3.48 (s, 2H), 3.75 (s, 3H), 7.02 (d, *J* = 8.7, 2H), 7.04–7.11 (m, 6H), 7.30–7.35 (m, 4H), 7.63–7.67 (m, 2H), 7.69 (s, 1H), 7.70 (s, 4H). HRMS (timsTOF) *m/z*: [M + H]⁺ Calcd for C₃₃H₃₅N₂O₂ 491.26930; Found 491.26850.

Slight Excess of *n*-butylamine

A mixture of MBH acetate **7** (50 mg, 0.105 mmol) in chloroform (10 mL) containing *n*-butylamine (0.016 mL, 0.162 mmol) was stirred at room temperature for 48 h. The reaction mixture was concentrated under reduced pressure and the resulting residue was purified by flash chromatography with the appropriate eluents to obtain the amine derivatives reported below (**9a,b**).

Dimethyl 2,2'-((butylazanediy)bis(methylene))bis(3-(4'-(diphenylamino)-[1,1'-biphenyl]-4-yl)acrylate) (**9b**)

Compound **9b** was obtained as a yellow glassy solid (17 mg, yield 36%) by using petroleum ether-ethyl acetate (9:1) as the eluent in the above flash chromatography purification. The ¹H NMR (400 MHz, DMSO-*d*₆) showed that compound **9b** was composed by a mixture of the diastereomers.

Methyl 2-((butylamino)methyl)-3-(4'-(diphenylamino)-[1,1'-biphenyl]-4-yl)acrylate (**9a**)

Compound **9a** (25 mg, yield 49%) was obtained as a yellow glassy solid as the most polar fraction by using petroleum ether-ethyl acetate (7:3) as the eluent in the above flash chromatography purification. The ¹H NMR (400 MHz, DMSO-*d*₆) showed that compound **9a** was composed by a mixture of (*E/Z*)-diastereomers in the ratio of about (74:26).

Reaction of MBHA Derivative **7** with *n*-butylamine Hydrochloride in Acetonitrile-Water-PBS

Large Excess of *n*-butylamine Hydrochloride

A mixture of MBH acetate **7** (50 mg, 0.105 mmol) in acetonitrile (12.5 mL), water (3.5 mL) containing solid PBS (Aldrich, 50 mg) and *n*-butylamine hydrochloride (58 mg, 0.529 mmol) was heated to reflux for 24 h. The reaction mixture was concentrated under reduced pressure and the resulting residue was partitioned between ethyl acetate and brine. The organic layer was dried under sodium sulfate and concentrated under reduced pressure. The resulting residue was purified by flash chromatography with the appropriate eluents to obtain the amine derivatives reported below (**9a,b**).

Dimethyl 2,2'-((butylazanediy)bis(methylene))bis(3-(4'-(diphenylamino)-[1,1'-biphenyl]-4-yl)acrylate) (**9b**)

Compound **9b** was obtained as a yellow glassy solid (25 mg, yield 52%) by using petroleum ether-ethyl acetate (9:1) as the eluent in the above flash chromatography purification. The ¹H NMR (400 MHz, DMSO-*d*₆) showed that compound **9b** was composed by a mixture of the diastereomers.

Methyl 2-((butylamino)methyl)-3-(4'-(diphenylamino)-[1,1'-biphenyl]-4-yl)acrylate (**9a**)

Compound **9a** (20 mg, yield 39%) was obtained as a yellow glassy solid as the most polar fraction by using petroleum ether-ethyl acetate (7:3) as the eluent in the above flash chromatography purification. The ¹H NMR (400 MHz, DMSO-*d*₆) showed that compound **9a** was composed by a mixture of (*E/Z*)-diastereomers in the ratio of about (93:7).

Slight Excess of *n*-butylamine Hydrochloride

A mixture of MBH acetate **7** (50 mg, 0.105 mmol) in acetonitrile (12.5 mL), water (3.5 mL) containing solid PBS (Aldrich, 50 mg) and *n*-butylamine hydrochloride (17 mg, 0.158 mmol) was heated to reflux for 24 h. The reaction mixture was concentrated under reduced pressure and the resulting residue was partitioned between ethyl acetate and brine. The organic layer was dried under sodium sulfate and concentrated under reduced pressure. The resulting residue was purified by flash chromatography with the appropriate eluents to obtain the amine derivatives reported below (**9a,b**).

Dimethyl 2,2'-((butylazanediy)bis(methylene))bis(3-(4'-(diphenylamino)-[1,1'-biphenyl]-4-yl)acrylate) (**9b**)

Compound **9b** was obtained as a yellow glassy solid (35 mg, yield 73%) by using petroleum ether-ethyl acetate (9:1) as the eluent in the above flash chromatography purification. The ¹H NMR (400 MHz, DMSO-*d*₆) showed that compound **9b** was composed by a mixture of the diastereomers.

Methyl 2-((butylamino)methyl)-3-(4'-(diphenylamino)-[1,1'-biphenyl]-4-yl)acrylate (**9a**)

Compound **9a** (8.0 mg, yield 16%) was obtained as a yellow glassy solid as the most polar fraction by using petroleum ether-ethyl acetate (7:3) as the eluent in the above flash chromatography purification. The ¹H NMR (400 MHz, DMSO-*d*₆) showed that compound **9a** was composed by a mixture of (*E/Z*)-diastereomers in the ratio of about (90:10).

Reaction of MBHA Derivative **7** with α -acetyl-L-lysine Methyl Ester Hydrochloride

A mixture of MBHA derivative **7** (67 mg, 0.14 mmol) in acetonitrile (12.5 mL) containing α -acetyl-L-lysine methyl ester hydrochloride (50 mg, 0.21 mmol), water (3.5 mL), and solid PBS (Aldrich, 25 mg) was refluxed for 24 h. The reaction mixture was concentrated under reduced pressure and the resulting residue partitioned between ethyl acetate and brine. The organic layer was dried over sodium sulfate and concentrated under reduced pressure. The final residue was purified by flash chromatography with the appropriate eluent to obtain the amino acid derivatives reported below (i.e. **9c** and **9d**).

Dimethyl 2,2'-(((5-acetamido-6-methoxy-6-oxohexyl)azanediy)bis(methylene))(S)-bis(3-(4'-(diphenylamino)-[1,1'-biphenyl]-4-yl)acrylate) (**9d**)

Compound **9d** was obtained as a yellow glassy solid (53 mg, yield 73%) by using ethyl acetate-petroleum ether (6:4) as the eluent in the above flash chromatography purification. The ¹H NMR (400 MHz, DMSO-*d*₆) spectrum showed that compound **9d** was composed by a mixture of the diastereomers. Samples of major diastereomer (*E,E*)-**9d** showing higher purities were obtained by further purification by flash chromatography. ¹H NMR (400 MHz, DMSO-*d*₆): 1.14–1.23 (m, 2H), 1.34–1.70 (m, 4H), 1.80 (s, 3H), 2.40 (t, *J* = 7.2, 2H), 3.50 (s, 4H), 3.53 (s, 3H), 3.70 (s, 6H), 4.12–4.16 (m, 1H), 6.93–7.00 (m, 4H), 7.01–7.12 (m, 12H), 7.28–7.37 (m, 8H), 7.50–7.58 (m, 8H), 7.71 (d, *J* = 8.3, 4H), 7.76 (s, 2H), 8.16 (d, *J* = 7.5, 1H). HRMS (timsTOF) *m/z*: [M + H]⁺ Calcd for C₆₇H₆₅N₄O₇ 1037.48478; Found 1037.48146.

Methyl *N*-acetyl-*N*'-(3-(4-(diphenylamino)-[1,1'-biphenyl]-4-yl)-2-(methoxycarbonyl)allyl)-L-lysinate (**9c**)

Compound **9c** (12 mg, yield 14%) was obtained as a yellow glassy solid as the most polar fraction by using ethyl acetate-methanol (9:1) as the eluent in the above flash chromatography purification. The ¹H NMR (400 MHz, DMSO-*d*₆) spectrum showed that compound **9a** was composed by a mixture of (*E/Z*)-diastereomers. Samples of major diastereomer (*E*)-**9c** showing purity higher than 97% were obtained by further purification by flash chromatography. ¹H NMR (400 MHz, DMSO-*d*₆) 1.28–1.46 (m, 4H), 1.50–1.71 (m, 2H), 1.81 (s, 3H), 2.53 (t, *J* = 6.6, 2H), 3.47 (s, 2H), 3.58 (s, 3H), 3.75 (s, 3H), 4.14–4.25 (m, 1H), 6.98–7.11 (m, 8H), 7.29–7.37 (m, 4H), 7.63–7.68 (m, 2H), 7.69 (s, 1H), 7.70 (s, 4H), 8.20 (d, *J* = 7.4, 1H). HRMS (timsTOF) *m/z*: [M + H]⁺ Calcd for C₃₈H₄₂N₃O₅ 620.31190; Found 620.31017.

Reaction of MBHA Derivative **7** with *n*-butyl-poly-(L-lysine) (BPLL)

Commercially available *n*-butyl-poly-(L-lysine) (BPLL) hydrochloride (Iris Biotech GmbH) (4.2 mg) was dissolved in deuterated dimethyl-sulfoxide (0.5 mL) into a 5 mm NMR tube and the appropriate amount of **7** (i.e. 2.0, 4.0, or 8.0 micromol) was added as a (50 mM) solution in DMSO-*d*₆. The resulting reaction mixture was promptly analyzed by recording a ¹H NMR spectrum to obtain the information on the starting conditions (*t* = 0). The tube was then heated into an oil bath at 50 °C and ¹H NMR spectra were recorded at regular time intervals (i.e. 1, 2, 4, 8, 24 h). The obtained spectra were elaborated all in the same manner and staked as shown in Figures SI-5, SI-6, SI-7.

The same experiments were repeated in the presence of suitable amounts (i.e. 2.0, 4.0, or 8.0 micromol) of DIPEA as the base (Figures SI-8, SI-9, SI-10).

Molecular Modelling

Calculations were performed using density functional theory (DFT) within the functional B3LYP with base 6–31 G* from the Gaussian16 package,^[61] in DCM and DMSO solutions. The Polarized Continuum Model (PCM) was used to simulate the solvent environment. Ground state geometry of **9b** was fully optimized using B3LYP/6–31 G* and Grimme dispersion D3 correction for long range interactions. Subsequently, absorption spectrum calculations were performed by the time-dependent (TD)DFT procedure, using the Coulomb-attenuated hybrid exchange-correlation functional (CAM–B3LYP) because it well describes structures with charge-transfer excited states.^[62,63] The same TD-DFT (CAM–B3LYP/6–31 G*) approach was used to calculate the optimized geometries of the emitting intermediates and the overall scheme of quantum chemical calculations of **9b**.

Photophysical Properties

UV-vis absorption spectra are obtained with a Perkin Elmer Lambda 900 spectrometer. PL spectra are obtained with with NanoLog composed by a iH320 spectrograph equipped with a Synapse QExtra charge-coupled device, by exciting with a monochromate 450 W Xe lamp. The spectra are corrected for the instrument response. PL QY values of solutions were obtained by using quinine sulfate as the reference. PL QY of solid casted films were measured with a home-made integrating sphere according to the procedure reported elsewhere.^[64] Time-resolved TCSPC measurements were obtained with PPD-850 single photon detector module by exciting with DD-405 L DeltaDiode Laser or DeltaTime series DD-300

DeltaDiode and analysed with the instrument Software DAS6. Average lifetimes are obtained by multiexponential fittings as $\tau_{av} = \sum_i \frac{A_i \tau_i^2}{A_i \tau_i}$

Photostability of Compounds **9a,b**

The solutions of compounds **9a,b** in deuterated dichloromethane contained into 5 mm NMR Pyrex tubes were irradiated with a monochromatic light centered at either 365 nm or 420 nm, and ¹H NMR spectra were recorded at regular time intervals (i.e. 0 min, 15 min, 30 min, 1, 2, 4, 8, and 24 h). A tunable light source Zolix (TLS2-X300PU–G, 300 W UV Xenon Light Source with monochromator Omni-λ2047i) was used for the irradiation of the solutions.

Dimethyl 3-butyl-6,7-bis(4-(diphenylamino)-[1,1'-biphenyl]-4-yl)-3-azabicyclo[3.2.0]heptane-1,5-dicarboxylate (**13**)

A solution of compound **9b** (25 mg, 27.5 micromol) in dichloromethane (3.75 mL) contained into a vial closed with a screw cap was irradiated with a monochromatic light centered at 420 nm by mean of a tunable light source Zolix (TLS2-X300PU–G, 300 W UV Xenon Light Source with monochromator Omni-λ2047i) at room temperature for 15 h. The reaction mixture was then concentrated under reduced pressure and the resulting residue was purified by flash chromatography with petroleum ether-dichloromethane (2:8) as the eluent to obtain compound **13** (14 mg, yield 56%) as an off-white solid. The ¹H NMR spectrum of the solid showed that compound **13** was composed by a mixture of diastereomers. For the sake of simplicity only the major diastereomer (**13-M**, Figure 9) was taken into consideration. ¹H NMR (600 MHz, CDCl₃): 0.91 (t, *J* = 7.2, 3H), 1.33–1.40 (m, 2H), 1.41–1.51 (m, 2H), 2.39 (d, *J* = 9.8, 1H), 2.41–2.47 (m, 1H), 2.57–2.63 (m, 1H), 2.73 (d, *J* = 9.7, 1H), 3.00 (d, *J* = 9.8, 1H), 3.29 (s, 3H), 3.42 (d, *J* = 9.6, 1H), 3.72 (s, 3H), 4.47 (d, *J* = 10.8, 1H), 4.80 (d, *J* = 10.8, 1H), 7.00–7.04 (m, 4H), 7.07–7.15 (m, 16H), 7.22–7.29 (m, 6H), 7.41–7.44 (m, 2H), 7.45–7.48 (m, 4H), 7.54 (d, *J* = 8.4, 2H), 7.58 (d, *J* = 8.4, 2H). ¹³C NMR (150 MHz, CDCl₃): 14.0, 20.5, 30.6, 44.0, 45.1, 51.3, 52.1, 54.5, 56.1, 57.9, 60.3, 63.0, 122.9, 124.0, 124.4, 126.3, 126.6, 127.0, 127.5, 127.7, 128.8, 129.3, 134.8, 135.0, 137.1, 138.3, 138.8, 139.2, 147.1, 147.7, 170.9, 175.0.

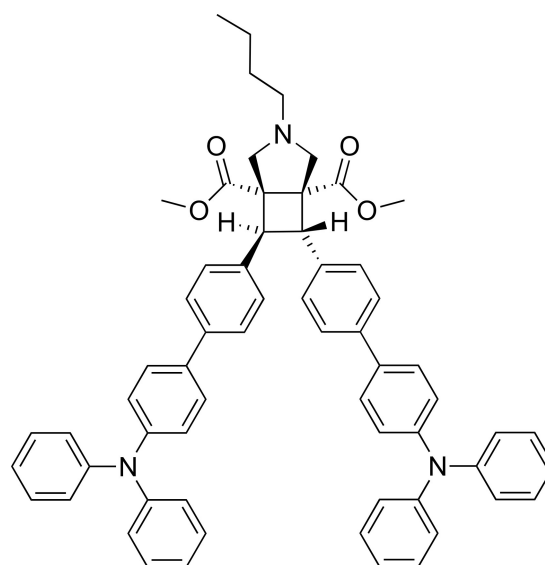


Figure 9. Probable structure of the major diastereomer **13-M** as suggested by NMR analysis. The structure of the corresponding enantiomer was omitted for the sake of simplification.

HRMS (timsTOF) m/z : $[M+H]^+$ Calcd for $C_{62}H_{58}N_3O_4$ 908.44218; Found 908.43915.

Acknowledgements

M.P. and A.C. acknowledge the MUR for the financial support under the project CN0000041 – “National Center for Gene Therapy and Drugsbased on RNA Technology” – CUP B63 C2200061 0006 Mission 4 Component 2 (M4 C2) – investment 1.4 [CN3] of the National Recovery and Resilience Plan (PNRR) funded by the European Union “Next Generation EU”. M.P. acknowledge the University of Siena for the financial support of the project Chromo-GENUP through the F-CUR2022 funding line (2265–2022-PM-CONRICMIUR_PC-FCUR2022_003). Open Access publishing facilitated by Università degli Studi di Siena, as part of the Wiley - CRUI-CARE agreement.

Conflict of Interests

The authors declare no conflict of interest.

Data Availability Statement

The data that support the findings of this study are available from the corresponding author upon reasonable request.

Keywords: Protein labeling · Fluorogenic labeling · Lysine · Morita–Baylis–Hillman Adduct · Cinnamic derivatives

- [1] V. K. Kadambar, A. Melman, *Adv. Exp. Med. Biol.* **2019**, *1140*, 237–250.
- [2] J. Maneesh, N. Kamal, S. K. Batra, *Trends Biotechnol.* **2007**, *25*, 307–316.
- [3] C. C. Ward, J. I. Kleinman, D. K. Nomura, *ACS Chem. Biol.* **2017**, *12*, 1478–1483.
- [4] P. Rosa-Neto, B. Wängler, L. Iovkova, G. Boening, A. Reader, K. Jurkschat, E. Schirmacher, *ChemBioChem* **2009**, *10*, 1321–1324.
- [5] V. Raindlová, R. Pohl, M. Hocek, *Chem. Eur. J.* **2012**, *18*, 4080–4087.
- [6] K. Pagano, M. Paolino, S. Fusi, V. Zanirato, C. Trapella, G. Giuliani, A. Cappelli, S. Zanzoni, H. Molinari, L. Ragona, M. Olivucci, *J. Phys. Chem. Lett.* **2019**, *10*, 2235–2243.
- [7] B. D. Smith, J. J. Higgin, R. T. Raines, *Bioorg. Med. Chem. Lett.* **2011**, *21*, 5029–5032.
- [8] S. B. Gunnoo, A. Madder, *ChemBioChem* **2016**, *17*, 529–553.
- [9] M. H. Mir, S. Parmar, C. Singh, D. Kalia, *Nat. Commun.* **2024**, *15*, 859.
- [10] V. Razzano, M. Paolino, A. Reale, G. Giuliani, R. Artusi, G. Caselli, M. Visintin, F. Makovec, A. Donati, F. Villafiorita-Monteleone, C. Botta, A. Cappelli, *ACS Omega* **2017**, *2*, 5453–5459.
- [11] V. Razzano, M. Paolino, A. Reale, G. Giuliani, A. Donati, G. Giorgi, R. Artusi, G. Caselli, M. Visintin, F. Makovec, S. Battiato, F. Samperi, F. Villafiorita-Monteleone, C. Botta, A. Cappelli, *RSC Adv.* **2018**, *8*, 8638–8656.
- [12] M. Paolino, A. Reale, V. Razzano, G. Giuliani, A. Donati, C. Bonechi, G. Caselli, M. Visintin, F. Makovec, C. Scialabba, M. Licciardi, E. Paccagnini, M. Gentile, L. Salvini, F. Tavanti, M. C. Menziani, A. Cappelli, *New J. Chem.* **2019**, *43*, 6834–6837.
- [13] M. Paolino, M. Visintin, E. Margotti, M. Visentini, L. Salvini, A. Reale, V. Razzano, G. Giuliani, G. Caselli, F. Tavanti, M. C. Menziani, A. Cappelli, *New J. Chem.* **2019**, *43*, 17946–17953.
- [14] G. Tassone, M. Paolino, C. Pozzi, A. Reale, L. Salvini, G. Giorgi, M. Orlandini, F. Galvagni, S. Mangani, X. Yang, B. Carloti, F. Ortica, L. Latterini, M. Olivucci, A. Cappelli, *ChemBioChem* **2022**, *23*, e202100449.
- [15] M. Saletti, M. Paolino, J. Venditti, C. Bonechi, G. Giuliani, A. Boccia, C. Botta, A. Cappelli, *Dyes Pigm.* **2023**, *219*, 111571.
- [16] M. Saletti, J. Venditti, M. Paolino, A. Zacchei, G. Giuliani, G. Giorgi, C. Bonechi, A. Donati, A. Cappelli, *RSC Adv.* **2023**, *13*, 35773–35780.
- [17] M. Saletti, M. Paolino, J. Venditti, C. Bonechi, G. Giuliani, S. Lamponi, G. Tassone, A. Boccia, C. Botta, L. Blancafort, F. Poggialini, C. Vagaggini, A. Cappelli, *ChemBioChem* **2024**, *25*, e202300862.
- [18] M. Lami, L. Barneschi, M. Saletti, M. Olivucci, A. Cappelli, M. Paolino, *ChemPhotoChem* **2024**, e202400093.
- [19] E. G. Guignet, R. Hovious, H. Vogel, *Nat. Biotechnol.* **2004**, *22*, 440–444.
- [20] B. A. Griffin, S. R. Adams, R. Y. Tsien, *Science* **1998**, *281*, 269–272.
- [21] B. Krishnan, A. Szymanska, L. M. Gierasch, *Chem. Biol. Drug Des.* **2007**, *69*, 31–40.
- [22] Z. Wang, X. Ding, S. Li, J. Shi, Y. Li, *RSC Adv.* **2014**, *4*, 7235–7245.
- [23] L. Rong, C. Zhang, Q. Lei, S.-Y. Qin, J. Feng, X.-Z. Zhang, *Adv. Sci.* **2016**, *3*, 1500211.
- [24] L. D. Lavis, T.-Y. Chao, R. T. Raines, *ACS Chem. Biol.* **2006**, *1*, 252–260.
- [25] J. Mei, N. L. C. Leung, R. T. K. Kwok, J. W. Y. Lam, B. Z. Tang, *Chem. Rev.* **2015**, *115*, 11718–11940.
- [26] D. Ding, K. Li, B. Liu, B. Z. Tang, *Acc. Chem. Res.* **2013**, *46*, 2441–2453.
- [27] W. C. Wu, C. Y. Chen, Y. Tian, S. H. Jang, Y. Hong, Y. Liu, R. Hu, B. Z. Tang, Y. T. Lee, C. T. Chen, W. C. Chen, A. K. Y. Jen, *Adv. Funct. Mater.* **2010**, *20*, 1413–1423.
- [28] A. Cappelli, G. P. Mohr, M. Anzini, S. Vomero, A. Donati, M. Casolaro, R. Mendichi, G. Giorgi, F. Makovec, *J. Org. Chem.* **2003**, *68*, 9473–9476.
- [29] A. Cappelli, M. Anzini, S. Vomero, A. Donati, L. Zetta, R. Mendichi, M. Casolaro, P. Lupetti, P. Salvatici, G. Giorgi, *J. Polym. Sci. Part A* **2005**, *43*, 3289–3304.
- [30] A. Cappelli, G. Pericot Mohr, G. Giuliani, S. Galeazzi, M. Anzini, L. Mennuni, F. Ferrari, F. Makovec, E. M. Kleinrath, T. Langer, M. Valoti, G. Giorgi, S. Vomero, *J. Med. Chem.* **2006**, *49*, 6451–6464.
- [31] A. Cappelli, S. Galeazzi, G. Giuliani, M. Anzini, A. Donati, L. Zetta, R. Mendichi, M. Aggravi, G. Giorgi, E. Paccagnini, S. Vomero, *Macromolecules* **2007**, *40*, 3005–3014.
- [32] A. Cappelli, S. Galeazzi, G. Giuliani, M. Anzini, M. Aggravi, A. Donati, L. Zetta, A. C. Boccia, R. Mendichi, G. Giorgi, E. Paccagnini, S. Vomero, *Macromolecules* **2008**, *41*, 2324–2334.
- [33] A. Cappelli, S. Galeazzi, G. Giuliani, M. Anzini, M. Grassi, R. Lapasin, G. Grassi, R. Farra, B. Dapas, M. Aggravi, A. Donati, L. Zetta, A. C. Boccia, F. Bertini, F. Samperi, S. Vomero, *Macromolecules* **2009**, *42*, 2368–2378.
- [34] A. Cappelli, M. Paolino, P. Anzini, G. Giuliani, S. Valenti, M. Aggravi, A. Donati, R. Mendichi, L. Zetta, A. C. Boccia, F. Bertini, F. Samperi, S. Battlato, E. Paccagnini, S. Vomero, *J. Polym. Sci. Part A* **2010**, *48*, 2446–2461.
- [35] A. Cappelli, M. Paolino, G. Grisci, G. Giuliani, A. Donati, R. Mendichi, A. C. Boccia, F. Samperi, S. Battiato, E. Paccagnini, E. Giacomello, V. Sorrentino, M. Licciardi, G. Giammona, S. Vomero, *Polym. Chem.* **2011**, *2*, 2518–2527.
- [36] A. Cappelli, M. Paolino, G. Grisci, G. Giuliani, A. Donati, R. Mendichi, A. C. Boccia, C. Botta, W. Mróz, F. Samperi, A. Scamporrino, G. Giorgi, S. Vomero, *J. Mater. Chem.* **2012**, *22*, 9611–9623.
- [37] A. Cappelli, G. Grisci, M. Paolino, F. Castriconi, G. Giuliani, A. Donati, S. Lamponi, R. Mendichi, A. C. Boccia, F. Samperi, S. Battiato, E. Paccagnini, M. Gentile, M. Licciardi, G. Giammona, S. Vomero, *Chem. Eur. J.* **2013**, *19*, 9710–9721.
- [38] A. Cappelli, M. Paolino, G. Grisci, G. Giuliani, A. Donati, A. C. Boccia, F. Samperi, R. Mendichi, S. Vomero, S., In *π -Stacked Polymers and Molecules*. Nakano T. Ed., Springer Japan: Osaka, **2014**, pp 51–149.
- [39] A. Cappelli, F. Villafiorita-Monteleone, G. Grisci, M. Paolino, V. Razzano, G. Fabio, G. Giuliani, A. Donati, R. Mendichi, A. C. Boccia, M. Pasini, C. Botta, *J. Mater. Chem. C* **2014**, *2*, 7897–7905.
- [40] A. Cappelli, G. Grisci, M. Paolino, V. Razzano, G. Giuliani, A. Donati, C. Bonechi, R. Mendichi, A. C. Boccia, M. Licciardi, C. Scialabba, G. Giammona, S. Vomero, *J. Mater. Chem. B* **2015**, *3*, 361–374.
- [41] W. Mróz, F. Villafiorita-Monteleone, M. Pasini, G. Grisci, M. Paolino, V. Razzano, A. Cappelli, C. Botta, *Mater. Lett.* **2015**, *142*, 197–200.
- [42] F. Villafiorita-Monteleone, A. Cappelli, M. Paolino, M. Colombo, E. Cariati, A. Mura, G. Bongiovanni, C. Botta, *J. Phys. Chem. C* **2015**, *119*, 18986–18991.
- [43] A. Cappelli, V. Razzano, M. Paolino, G. Grisci, G. Giuliani, A. Donati, R. Mendichi, F. Samperi, S. Battiato, A. C. Boccia, A. Mura, G. Bongiovanni, W. Mróz, C. Botta, *Polym. Chem.* **2015**, *6*, 7377–7388.
- [44] A. Cappelli, V. Razzano, G. Fabio, M. Paolino, G. Grisci, G. Giuliani, A. Donati, R. Mendichi, W. Mróz, F. Villafiorita-Monteleone, C. Botta, *RSC Adv.* **2015**, *5*, 101377–101385.

- [45] A. Cappelli, M. Paolino, G. Grisci, V. Razzano, G. Giuliani, A. Donati, C. Bonechi, R. Mendichi, S. Battiato, F. Samperi, C. Scialabba, G. Giammona, F. Makovec, M. Licciardi, *Polym. Chem.* **2016**, *7*, 6529–6544.
- [46] F. Villafiorita-Monteleone, E. Kozma, M. Pasini, M. Paolino, A. Cappelli, G. Bongiovanni, A. Mura, C. Botta, *Appl. Phys. Lett.* **2017**, *110*, 183301.
- [47] F. Villafiorita-Monteleone, E. Kozma, U. Giovanella, M. Catellani, M. Paolino, V. Collico, M. Colombo, A. Cappelli, C. Botta, *Dyes Pigm.* **2018**, *149*, 331–335.
- [48] F. Fabrizi de Biani, A. Reale, V. Razzano, M. Paolino, G. Giuliani, A. Donati, G. Giorgi, W. Mróz, D. Piovani, C. Botta, A. Cappelli, *RSC Adv.* **2018**, *8*, 10836–10847.
- [49] M. Paolino, G. Grisci, A. Reale, V. Razzano, G. Giuliani, A. Donati, R. Mendichi, D. Piovani, A. Boccia, A. Grillo, G. Giorgi, A. Cappelli, *Polymers (Basel)*. **2018**, *10*, 752.
- [50] M. Paolino, G. Grisci, F. Castriconi, A. Reale, G. Giuliani, A. Donati, C. Bonechi, G. Giorgi, R. Mendichi, D. Piovani, A. C. Boccia, M. Canetti, F. Samperi, S. Dattilo, C. Scialabba, M. Licciardi, E. Paccagnini, M. Gentile, A. Cappelli, *Pharmaceutica* **2018**, *10*, 234.
- [51] M. Paolino, A. Reale, V. Razzano, G. Giuliani, A. Donati, G. Giorgi, A. C. Boccia, R. Mendichi, D. Piovani, C. Botta, L. Salvini, F. Samperi, C. Savoca, M. Licciardi, E. Paccagnini, M. Gentile, A. Cappelli, *Pharmaceutica* **2019**, *11*, 444.
- [52] M. Paolino, A. Reale, G. Magrini, V. Razzano, G. Giuliani, A. Donati, G. Giorgi, F. Samperi, M. Canetti, M. Mauro, F. Villafiorita-Monteleone, E. Fois, C. Botta, A. Cappelli, *Eur. Polym. J.* **2020**, *137*, 109923.
- [53] M. Paolino, A. Reale, G. Magrini, V. Razzano, M. Saletti, G. Giuliani, A. Donati, F. Samperi, A. Scamporrino, M. Canetti, M. Mauro, F. Villafiorita-Monteleone, E. Fois, C. Botta, A. Cappelli, *Eur. Polym. J.* **2021**, *156*, 110597.
- [54] M. Paolino, M. Saletti, A. Reale, V. Razzano, G. Giuliani, A. Donati, C. Bonechi, G. Giorgi, A. Atrei, M. Mauro, A. Scamporrino, F. Samperi, E. Fois, G. Tabacchi, C. Botta, A. Cappelli, *Eur. Polym. J.* **2022**, *169*, 111137.
- [55] M. Paolino, M. Saletti, A. Reale, M. Licciardi, P. Varvarà, A. Marquette, J. Léonard, C. Bonechi, A. Donati, G. Giorgi, G. Giuliani, B. Carlotti, F. Ortica, L. Latterini, M. Gentile, E. Paccagnini, M. Olivucci, A. Cappelli, *Chem. Eur. J.* **2022**, *28*, e202201477.
- [56] M. Paolino, M. Saletti, A. Reale, V. Razzano, G. Giuliani, A. Donati, C. Bonechi, G. Giorgi, G. Mercorillo, F. Samperi, W. Mróz, C. Botta, A. Cappelli, *Eur. Polym. J.* **2023**, *189*, 111957.
- [57] M. Paolino, A. Reale, V. Razzano, G. Giorgi, G. Giuliani, F. Villafiorita-Monteleone, C. Botta, C. Coppola, A. Sinicropi, A. Cappelli, *New J. Chem.* **2020**, *44*, 13644–13653.
- [58] A. Nangia, G. R. Desiraju, *Chem. Commun.* **1999**, 605–606.
- [59] K. J. Kunal, K. Anil, M. Parthapratim, *Cryst. Growth Des.* **2023**, *23*, 2922–2931.
- [60] R. Improta, F. Santoro, L. Blancafort, *Chem. Rev.* **2016**, *116*, 3540–3593.
- [61] *Gaussian 16*, Revision C.01, M. J. Frisch, G. W. Trucks, H. B. Schlegel, G. E. Scuseria, M. A. Robb, J. R. Cheeseman, G. Scalmani, V. Barone, G. A. Petersson, H. Nakatsuji, X. Li, M. Caricato, A. V. Marenich, J. Bloino, B. G. Janesko, R. Gomperts, B. Mennucci, H. P. Hratchian, J. V. Ortiz, A. F. Izmaylov, J. L. Sonnenberg, D. Williams-Young, F. Ding, F. Lipparini, F. Egidi, J. Goings, B. Peng, A. Petrone, T. Henderson, D. Ranasinghe, V. G. Zakrzewski, J. Gao, N. Rega, G. Zheng, W. Liang, M. Hada, M. Ehara, K. Toyota, R. Fukuda, J. Hasegawa, M. Ishida, T. Nakajima, Y. Honda, O. Kitao, H. Nakai, T. Vreven, K. Throssell, J. A. Montgomery, Jr., J. E. Peralta, F. Ogliaro, M. J. Bearpark, J. J. Heyd, E. N. Brothers, K. N. Kudin, V. N. Staroverov, T. A. Keith, R. Kobayashi, J. Normand, K. Raghavachari, A. P. Rendell, J. C. Burant, S. S. Iyengar, J. Tomasi, M. Cossi, J. M. Millam, M. Klene, C. Adamo, R. Cammi, J. W. Ochterski, R. L. Martin, K. Morokuma, O. Farkas, J. B. Foresman, and D. J. Fox, Gaussian, Inc., Wallingford CT, **2016**.
- [62] A. D. Becke, *J. Chem. Phys.* **1993**, *98*, 5648–5652.
- [63] C. Lee, W. Yang, R. G. Parr, *Phys. Rev. B* **1988**, *37*, 785–789.
- [64] J. Moreau, U. Giovanella, J.-P. Bombenger, W. Porzio, V. Vohra, L. Spadacini, G. Di Silvestro, L. Barba, G. Arrighetti, S. Destri, M. Pasini, M. Saba, F. Quochi, A. Mura, G. Bongiovanni, M. Fiorini, M. Uslenghi, C. Botta, *ChemPhysChem* **2009**, *10*, 647–653.

Manuscript received: May 30, 2024

Revised manuscript received: July 12, 2024

Accepted manuscript online: July 23, 2024

Version of record online: September 21, 2024